Transmission Line Modeling and Synthesis for Multi-Channel Communication *

Jun Chen and Lei He
Electrical Engineering Department,
University of California, Los Angeles, 90095

ABSTRACT

To overcome the limitations of traditional interconnects, transmission lines that transmit multi-channel signals via high frequency carriers have recently been proposed and realized for intra-chip and inter-chip communication. We derive a closed-form model for SNR for such interconnects with multiple ports and branches, and propose efficient figures of merit (FOMs) to minimize signal distortion. Experiments show that the SNR model is accurate compared to SPICE simulation and signal distortion FOMs are effective. Using the proposed models, we further automatically synthesize coplanar waveguides for radio-frequency (RF) interconnects with capacitive couplers. We minimize the total interconnect area under constraints of SNR and signal distortion. Compared to the published manual designs, the synthesized solution can reduce up to 80% area. Furthermore, the optimized solutions vary greatly with respect to number of ports, frequency bands, topologies and terminations, and therefore automatic synthesis is needed.

1. INTRODUCTION

Transmission lines have long been used in on-board and in-package communication. For on-chip communication, traditional interconnects transmit baseband signals and are RC dominant. They have inherent signal distortion and large RC delay [1], and the delay can not scale as well as transistor speed. Recently transmission lines have also been proposed in the literature for high speed and high bandwidth on-chip communication. One kind of such interconnects such as [2, 4, 6, 7] directly transmit baseband signal. Their transceivers are simple, but they have limited wire bandwidth because the interconnect is wide but hard to be shared between different transceivers. Besides, they operate at base band and have similar limitations as traditional interconnects. Another kind of interconnects such as [3, 5, 1] modulates the baseband signal before transmission with high frequency carrier such as RF signal. The signals in such interconnects are transmitted in high frequency bands which have much smaller distortion and can be propagated at a velocity close to the speed of light [1]. Another advantage of such interconnects is that they can be shared by multiple communication channels at different frequency bands, and each frequency band can be further shared by multiple code-division communication channels. Therefore the interconnect potentially can have large bandwidth and also reconfigurable. In this paper, we focus on this type of multi-channel interconnects.

Prototypes of interconnects transmitting signals via high frequency carriers have already been presented in [3, 5, 8, 1]. All these prototypes are designed manually. Manual design takes time and may result in unnecessarily wide wires as we will see later in this paper. On the other hand, system-scale designs such as in [5, 7] are too complex to design manually. To bridge this gap, more efficient model and automatic synthesis methods are needed, and an accurate model must consider multiple channels, multiple ports and branches. In addition, because of the analog nature of the carrier and transceivers, the model should focus on the frequency-dependent signal to noise ratio (SNR) and signal distortion.

Numerical methods such as circuit simulation e.g. [9] and model order reduction e.g. [10] provide generic solutions to the voltage response in time or frequency domain, but they are too time consuming to be used in automatic synthesis. Analytic methods are efficient and can be used in synthesis. However, existing analytic models e.g. [11] focus on delay and noise in time domain (and for only two ports), and there exists no analytical model for frequency-dependent SNR and signal distortion in a multi-port transmission line.

In this paper, we present efficient models for transmission lines with high frequency carriers and multiple frequency channels, multiple ports and branches. We first derive an accurate model with linear complexity for the frequency-domain voltage response in branched transmission lines and then develop closed-form formulas for the amplitude of the signal and the reflection noise at receivers. We thus obtain the frequency-dependent SNR for each receiver. The SNR model is accurate compared to SPICE simulations. We also propose figures of merit (FOMs) to minimize the signal distortion in both signal phase and amplitude. The proposed SNR model and distortion FOMs can be applied to any multi-band multi-port transmission lines with high frequency carriers. As an example, we apply our models to synthesis of coplanar waveguide (CPW) for on-chip multi-channel radio-frequency (RF) communication under constraints of SNR and signal distortion. We minimize the area of the interconnects with either perfect or imperfect terminations. The synthesis results demonstrate up to 80% less chip area compared to the published manual designs [3]. We also successfully synthesize an interconnection with multiple branches. All the designs have been verified with time-domain transient simulation, which further validates our models. The synthesized designs vary with respect to the topologies, the number of ports, frequency bands and terminations, and therefore show the effectiveness and necessity of the automatic synthesis process.

The rest of the paper is organized as follows: In section 2 we present the model for SNR and FOMs of signal distortion for multi-port transmission lines. In section 3 we automatically synthesize CPW structure for RF interconnection. We

---

conclude the paper in section 4.

2. MODELS FOR MULTI-PORT TRANSMISSION LINES

In this section, we develop the models for multi-port branched transmission line. We assume the signal is transmitted via a carrier signal at a fixed frequency and develop our models in frequency domain. To avoid ambiguity, in this work we define a frequency channel as a FDMA (frequency division multiple access) channel with a fixed carrier frequency, and a communication channel as a signal path from a transmitter to a receiver. Each communication channel has only one transmitter and one receiver. Each frequency channel can only have one transmitter, but it may have multiple receivers, and therefore can include multiple communication channels. We first show an accurate model for port voltage response, and then we develop a closed-form model for SNR of branched transmission line structures. In addition, we propose metrics for signal distortion.

2.1 Background of Transmission Line

A transmission line can be described as,

$$\frac{\partial V}{\partial x} = -(R + j\omega L)I \tag{1}$$

$$\frac{\partial I}{\partial x} = -(G + j\omega C)V \tag{2}$$

Where, R, L, G and C are the unit length resistance, inductance, conductance and capacitance of the transmission line. G is usually very small and can be ignored. The characteristic impedance of the transmission line is,

$$Z_0 = \sqrt{\frac{R + j\omega L}{G + j\omega C}} \tag{3}$$

The general solution to (1) and (2) is

$$V = A \exp(-\gamma x) + B \exp(\gamma x) \tag{4}$$

$$I = A/Z_0 \exp(-\gamma x) - B/Z_0 \exp(\gamma x) \tag{5}$$

where A and B are determined by boundary conditions. In (4) and (5) the component of $\exp(-\gamma x)$ is the forward wave propagating in the positive direction of x axis, and the component $\exp(\gamma x)$ is the backward wave propagating in the negative direction of x axis. γ is the propagation constant of the transmission line and is defined as

$$\gamma = \sqrt{(R + j\omega L)(G + j\omega C)} \tag{6}$$

The propagated wave is reflected at the terminations of the line. Assuming the impedance of the termination is Z_t, and the amplitudes of forward and backward waves are A and B, then the reflection ratio is

$$\Gamma = \frac{B}{A} = \frac{Z_0 - Z_t}{Z_0 + Z_t} \tag{7}$$

Reflections constitute part of the noise interfering with the propagated signal.

2.2 Port Voltage Response

Multiple branches and ports connected to the transmission line introduce extra discontinuities and reflections. In Figure 1, we show the interconnect model with multiple transceivers and branches. We assume linear transmitter and receiver models, and model each of them uniformly with
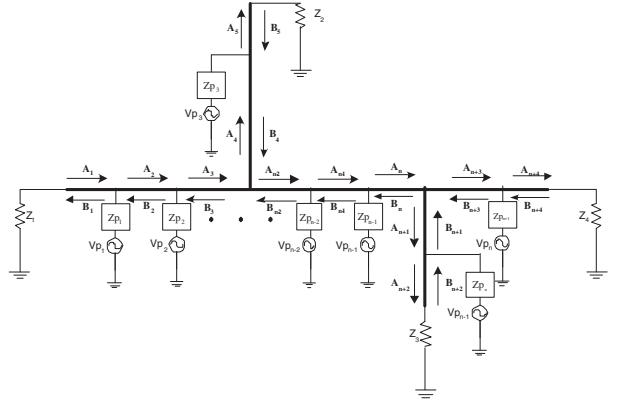
Figure 1: Circuit model of multi-port transmission line

a lumped impedance and an AC voltage source, where the amplitude of the voltage source for a receiver is zero. The capacitive coupler is modeled as a lumped capacitor. Because the circuit is linear, according to superposition principle we can consider each frequency channel separately.

We consider three types of discontinuities of the transmission line structure: ports, branching points and terminations. The segment between adjacent discontinuities is a continuous segment of transmission line, where the general solution of (4) and (5) still holds. The current and voltage between adjacent discontinuities k and $k + 1$ can be written as

$$V_k(x) = A_k \exp(-\gamma(x - x_k)) + B_k \exp(\gamma(x - x_{k+1})) \tag{8}$$

$$I_k(x) = \frac{A_k}{Z_0} \exp(-\gamma(x - x_k)) - \frac{B_k}{Z_0} \exp(\gamma(x - x_{k+1})) \tag{9}$$

where A_k and B_k are the amplitudes of the forward and backward waves (see Figure 1), Z_0 is the characteristic impedance of the transmission line and x_k is the location of discontinuity k. A_k and B_k are unknown variables to be determined by our voltage response model.

Each transmitter or receiver is a *port* to the interconnect. At a port k, by applying the KVL and KCL we have

$$V_k(x_k) = V_{k+1}(x_k) \tag{10}$$

$$Zp_k(I_k(x_k) - I_{k+1}(x_k)) = V_k(x_k) - Vp_k(x_k) \tag{11}$$

where Zp_k is the transceiver impedance and Vp_k is the transceiver voltage at port k.

At a branching point with n branches connected, we have incoming waves (A_i) and outgoing waves (B_i) on each connected branches, where $i = 1, 2, \ldots, n$. According to KCL,

$$\sum_{i=1}^{n} (A_i/Z_i - B_i/Z_i) = 0 \tag{12}$$

where Z_i is the characteristic impedance of branch i. Also because the branches are connected at the branching point, for any pair of branches i and j,

$$A_i + B_i = A_j + B_j \tag{13}$$

At the terminations of the transmission line, the voltage and current of the transmission line must satisfy the following equation

$$V = Z_t I \tag{14}$$

95
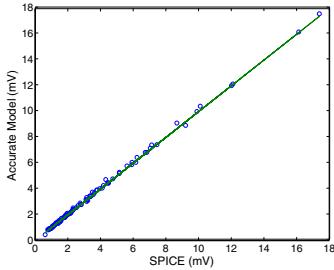
Figure 2: Voltage comparison between model in section 2.2 and SPICE simulation

Assuming there are n ports and b branches, then there are $n + b$ segments of transmission lines and totally $2(n+b)$ unknown variables. (10)-(14) give $2n + 2b$ linear equations. Because only neighboring segments have coupling terms, the matrix is a sparse band matrix, the equation set can be efficiently solved by Gaussian elimination method with a time complexity of $O(n)$. We compare our voltage response model with SPICE simulations in Figure 2 for the voltage amplitude at different receivers. All SPICE simulations in this paper use a distributed RLC model with one RLC circuit for each wire segment of $5\mu m$. Other settings such as transceiver impedances and locations are randomly generated. The number of ports is between 10 and 100, and we randomly choose the communication channel for comparison. According to the figure, our model almost perfectly matches the SPICE simulations.

2.3   SNR Model

To facilitate the computation of SNR and distortions, we develop models for signal and reflection noise amplitude at the receiver of one communication channel. Obviously each transmitter or receiver can only transmit signals on one frequency channel. Signals in other channels are filtered out by the receiver. Based on superposition principle, we can compute the waveform of each frequency channel separately. We assume the transceiver impedances are much larger than Z_0 so that the reflections from the ports are small and the transmission line is not disturbed much by the shunt impedances. With this assumption, we first derive a simplified model considering only the transmitter and the receiver in an unbranched transmission line without branches and ignoring other ports and terminations, and then extend the model to consider the effects of other ports, termination reflections and branching points.

2.3.1   Isolated Communication Channel

In this subsection, we consider one transmitter and one receiver on an unbranched transmission line without branches and ignore the effect of other ports and terminations. We also only consider first order effects on the signal at the receiver, which means we only consider the reflected wave from only one reflection, because waves after multiple reflections will have very small amplitudes. Under these assumptions, following the same notation as in section 2.2 and assuming the transmitter at port 1 and the receiver at port 2, the simplified model for the transmitter port and the receiver port are shown in Figure 3. According to (8)-(11), at the transmitter port we obtain

$$A_2 = \frac{Z_0/2}{Z_0/2 + Z_s} V_s \qquad (15)$$
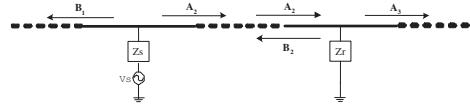
Figure 3:   Simple model for transmitter and receiver port

where Z_s and V_s are the impedance and voltage at transmitter port. B_2 is ignored at the transmitter port because we only consider the first order effect on the signal at the receiver. Similarly, at the receiver we have

$$A_3 = \frac{2A_2}{Z_0/Z_r + 2} \exp(-\gamma\ell) \qquad (16)$$

$$B_2 = -\frac{A_2}{1 + 2Z_r/Z_0} \exp(-\gamma\ell) \qquad (17)$$

where Z_r is the shunt impedance at the receiver port, and ℓ is the distance between the transmitter and the receiver. A_3 is the signal after the reflection at the receiver port. Since A_2 has been solved in (15), the voltage across receiver input resistance R_r is

$$V_r = \frac{R_r}{Z_r} A_3 = \frac{R_r Z_0/2}{(Z_0/2 + Z_r)(Z_0/2 + Z_s)} \exp(-\gamma\ell)V_s \quad (18)$$

which is the signal voltage at the receiver.

2.3.2   Effect of Multiple Ports

In this section, we further consider the effect of other ports and extend the model in section 2.3.1. When a propagating wave passes through a port, part of the signal is reflected according to (16) and (17). The situation is similar to that at a receiver in section 2.3.1. According to (16), the transmission rate for port k is

$$\xi_k = \frac{2}{Z_0/Zp_k + 2} \qquad (19)$$

where Zp_k is the impedance of port k. According to (17), the reflection rate for port k is,

$$\rho_k = -\frac{1}{1 + 2Zp_k/Z_0} \qquad (20)$$

Obviously, when Zp_k is large compared to Z_0, ξ_k is close to 1 and ρ_k is close to 0.

2.3.3   Effect of Terminations

According to (7), when the terminations are equal to the characteristic impedance Z_0, there will be no reflection from the terminations. Although the perfect termination may be designed, the terminations may be different from the ideal case because of the process variations. Imperfect terminations cause reflection and introduce extra noise. For terminations, we only concerns about the reflection noise. According to (7), the reflection coefficient of a termination with a lumped impedance of Z_t is,

$$\rho_t = \Gamma = \frac{Z_0 - Z_t}{Z_0 + Z_t} \qquad (21)$$

2.3.4   Effect of Branch Junctions

In this section, we further extend our model to consider branched interconnections. A branched interconnection has *junctions* or *branching points* connecting two or more uniform interconnects.   These junctions introduce extra dis-
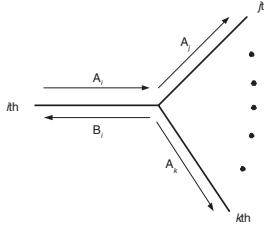
Figure 4: Circuit model of multi-port transmission line

continuity to the signal, and cause more loss of signal and reflection noise.

To consider the effects of junctions, we need to compute the signal transmission rate and reflection rate of each branch at the junction. Considering a junction connecting n branches, let the characteristic impedance of ith branch connected to the junction be Z_{0i}. For the a signal traveling on ith branch towards the junction, part of the signal will be reflected due to the discontinuity and the rest will be transmitted to other branches. Since we will consider reflections from other discontinuity separately and temporarily ignore them, the signals on all the branches are shown in Figure 4. Using KCL and KVL, the reflection rate for branch i is derived as,

$$\rho_i = \frac{Z_{ti} - Z_{0i}}{Z_{ti} + Z_{0i}} \tag{22}$$

where,

$$Z_{t,i} = \frac{1}{\sum_{j \neq i} 1/Z_{0j}} \tag{23}$$

The transmission rate is,

$$\xi_i = \frac{2Z_{ti}}{Z_{ti} + Z_{0i}} \tag{24}$$

2.3.5 SNR

With the transmission and reflection rates of the discontinuities, including ports, junctions and terminations, the signal received by receiver r from transmitter s is derived as,

$$V_s = k_{s,r} \prod_{i \in s \to r, i \neq s} \exp(-l_{i-1,i}\gamma_{i-1,i})\xi_i \tag{25}$$

where $s \to r$ is the shortest path from s to r. $l_{i-1,i}$ is the branch length between $(i-1)$th discontinuity and ith discontinuity, $\gamma_{i-1,i}$ is the propagation constant of the branch, and ξ_i is the ith discontinuity's transmission rate. $k_{s,r}$ is a coefficient depending on the transmitter, and is defined as

$$k_{s,r} = \frac{R_r Z_{0r}/2V_s}{(Z_{0s}/2 + Z_s)(Z_{0r}/2 + Z_r)} \tag{26}$$

where R_r is the receiver input resistance, and Z_{0s} and Z_{0r} are the characteristic impedance of the branches where transmitter and the receiver are located respectively.

Because we require small reflection rate for large SNR, higher order reflections result in negligible noise. Therefore, to compute the reflection noise from ports, we only consider the first order reflection. With all the discontinuities, the first order reflection noise at the receiver r from transmitter
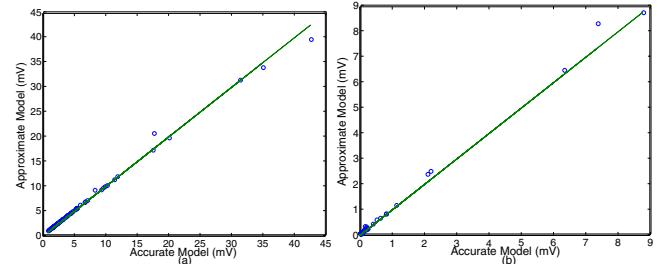
Figure 5: Comparison between numerical solution in section 2.2 and (a) formula (25) for signal at receivers; (b) formula (27) for reflection noise from ports

s is,

$$\begin{aligned} V_n &= k_{s,r} \sum_p \left(\prod_{i \in s \to p, i \neq s} \exp(-l_{i-1,i}\gamma_{i-1,i})\xi_i \cdot \rho_p \right. \\ &\quad \left. \cdot \prod_{j \in p \to r, j \neq s} \exp(-l_{j-1,j}\gamma_{j-1,j})\xi_j \right) \end{aligned} \tag{27}$$

where discontinuity p is a discontinuity not on the shortest path from s to r, and ρ_p is the reflection rate of pth discontinuity.

(25) and (27) are verified by comparing with the results derived from the accurate model in section 2.2. The setting is randomly generated and the results are shown in Figure 5. From the figures, we can see the models are highly accurate compared to the numerical solution.

The signal at the receiver node is given in (25). The SNR at a receiver can be computed as,

$$\mathbf{SNR} = 10 \log \frac{\frac{V_s^2}{2R_r}}{\frac{V_n^2}{2R_r} + P_n} \tag{28}$$

where P_n is the power of the intrinsic receiver noise.

2.4 Metrics of Signal Distortion

The distortion of the waveform depends on attenuation and phase delay. The attenuation is defined as the reduction of the signal amplitude compared to the original signal. The phase delay is defined as

$$P(\omega) = -\frac{\Delta\phi(\omega)}{\omega} \tag{29}$$

where $\Delta\phi$ is the frequency dependent phase changing compared to the original signal and ω is the radial frequency of the carrier. A distortionless communication channel should have attenuation and phase delay, both uniform over the frequency band for a frequency channel.

To ensure small distortion we require limited difference of phase delay and attenuation in a frequency channel,

$$\Delta P = \frac{|P(\omega_0 - \omega_b) - P(\omega)|}{T_b} < 0.01 \tag{30}$$

$$\Delta M = \frac{|M(\omega_0 - \omega_b) - M(\omega_0)|}{M(\omega_0)} < 0.01 \tag{31}$$

where ω_0 is the carrier frequency, ω_b is the digital baseband frequency, and T_b is the baseband period. The phase P and amplitude M are computed according to (25). (30) and (31) are our FOM for signal distortion.
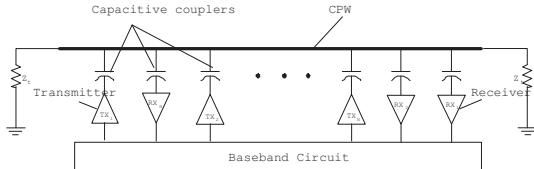
Figure 6: On-chip RF interconnection structure

3. SYNTHESIS OF CPW

In this section, we apply these models to optimize the area of CPW-typed RF interconnection with multiple transceivers and multiple carriers. Due to the limited space, we briefly present our experiment results. More details and experiment results will be presented in a technique report.

3.1 Radio-Frequency Interconnects

The prototypes of multi-channel radio-frequency interconnection have been shown in [3, 8]. As shown in Figure 6 of an on-chip RF interconnect, the digital signal is first mixed with an RF carrier by a transmitter, and then coupled via a capacitive coupler into the interconnect, which is a transmission medium such as a coplanar waveguide (CPW) or a microstrip transmission line (MTL). The RF signal is transmitted bidirectionally along the interconnect, and picked up by multiple receivers via capacitive couplers and demodulated to obtain the original digital signal. An RF interconnects can be shared by multiple transmitters.

For CPW, we denote the signal wire width as w, the shielding wire width as g, and spacing between signal and shielding wires as s. We extract frequency-dependent resistance and partial inductance with FastHenry [12] and calculate the capacitance by the formula of $C = 1/(c^2 L)$, where uniform dielectric is assumed and c is the speed of light. The capacitive couplers of transceivers are modeled by lumped capacitors, and the transceivers are modeled by linear drivers.

3.2 Automatic Synthesis

We assume that the transceivers have been given and the noise characteristics of the receivers are determined beforehand. We formulate the problem as below,

FORMULATION 1. *Given the transceivers and the noise characteristics of receivers P_n (see (28)) , determine the signal wire width w, signal-shield spacing s, shielding width g, and the size of each capacitive coupler such that the total area of the interconnect and capacitive couplers is minimized under the constraint that at each receiver our FOM (30) and (31) for signal distortion are satisfied, and SNR is larger than the required minimum SNR.*

Our closed-form models in (28), (30) and (31) enable us to use simulated annealing (SA) algorithm to optimize the wire geometries and the size of each capacitive coupler in a relatively short run time. The detailed objective function and process is omitted here due to limited space and will be provided in a technique report.

3.3 Experiment Results

3.3.1 Perfect Terminations

We first assume that the interconnection is unbranched and the terminations are perfect and therefore there is no re-

Table 1: Comparison between manual design and automatic synthesis

design	w	s	g	total width	C_s	C_r
manual	-	-	-	$100\mu m$	100fF	100fF
synthesis	$2.2\mu m$	$6.0\mu m$	$1.1\mu m$	$16.8\ \mu m$	51fF	49fF
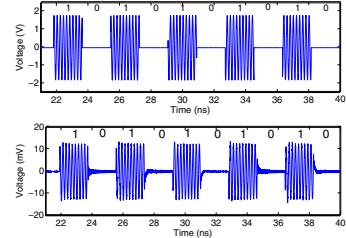
Figure 7: Transient waveform. (a) upper: Input; (b) lower: Output

flection from the terminations. For comparison we first synthesize an RF interconnect with the same specifications as in [3]. The interconnect length is $1cm$, the carrier frequency is 5GHz, the baseband frequency is 275MHz, the transceiver impedance is 2kΩ, the transmitter voltage is 1.8V and the power of receiver intrinsic noise is -67dBm. The minimum SNR is set to 20dB. One transmitter and one receiver are at the opposite ends of the interconnect. As shown in Table 1 the synthesis result reduces the total interconnect width including spacing by 80% and the coupler size by 50% compared to manual design in [3]. Figure 7 plots input and output waveforms with clear repeated "01" pattern. The signal amplitude is $14mV$ and therefore the SNR is 21dB which satisfies the lower bound constraint of 20dB.

3.3.2 Imperfect Terminations

In reality, the terminations are often mismatched due to process variations. In this section, we study the impact of imperfect terminations on the synthesis results. The RF interconnection under study is 1cm long with 5 channels allocated from 10 to 110 GHz with 20GHz for each channel. Each channel has 1 transmitter and 4 receivers. The locations of the ports are randomly selected. The lower bound of SNR is set to 15dB. We define the mismatch degree as the relative difference between the real termination and the perfect termination. Figure 8 shows the trend of the interconnect area and coupler size with the increasing of different degrees of mismatch. It is clear the total interconnect area increases with the increasing of mismatch. The coupler size has the similar trends but with much smaller slope. When the mismatch is larger than 15%, no valid solutions are found.
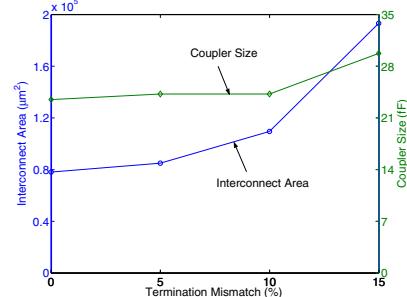
Figure 8: Interconnect area and coupler size with different termination mismatch.
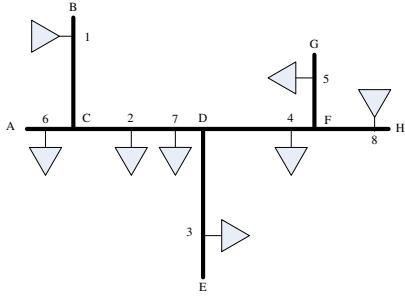
Figure 9: A sample structure of branched RF interconnects.

Table 2: Geometries of each CPW segment.

branch	length(μm)	w(μm)	s(μm)	g(μm)	area (μm^2)
AC	1000	0.5	5.1	0.1	10900
BC	5000	2.7	6.1	1.5	89500
CD	5000	5.8	2.3	2.3	75000
DE	6000	1.8	6.1	0.9	94800
DF	4000	6.4	3.4	2.2	70400
FG	3000	0.8	8.0	0.3	52200
FH	2000	2.3	10	1.1	90400

3.3.3 Branched Interconnection

We synthesize an RF interconnection with branches in this section. In this experiment, the impedances of all the transceivers are 1000Ω and we assume perfect terminations. The minimum SNR is set to 15dB. The transmitter input voltage is 1.8v. In Figure 9 we show one example of branched RF interconnects. The structure has one main interconnect branch and three sub branches. Segments AC, CD, DF and FH can have different optimal geometries. There are two channels. Channel 1 is at 10GHz and has four receivers at port 2, 3, 4 and 5 receiving signal from the transmitter at port 1. Channel 2 is at 20GHz and has two receivers at port 6 and 7 receiving signal from the transmitter at port 8. Table 2 shows the synthesized geometries of each segment and table 3 shows the synthesized value of the coupling capacitor at each port. From the results we can see the synthesized values for each segments are different. For segments shared by signal paths such as CD and DF, signal wire width and shield width are large to reduce the attenuation of the signal. Sub-branch segments have smaller signal width and shield width, but the spacing between them can be large to match the impedance at the branching points. For each channel, the transmitter has the largest coupling capacitor compared to receivers, and receivers farther from the transmitters has larger coupling capacitors than those closer to the transmitters.

We further carry out SPICE simulation to verify the results. The amplitudes of signal at each receiver from both SPICE simulation and the proposed model are shown in table 3. We can see the results of our model closely match those from SPICE simulation.

4. CONCLUSION AND DISCUSSIONS

Multi-channel multi-port transmission lines that transmit signals via high-frequency carriers have been used for high-

speed high-bandwidth intra-chip and inter-chip communications. To efficiently analyze and design such transmission line, we first developed an efficient model with linear complexity to compute the voltages of multi-port transmission line, and then derived closed-form models for SNR at receivers. We also proposed figures of merit to minimize the distortion in signal phase and amplitude. Experiments show that the SNR model is accurate compared to SPICE simulation and signal distortion FOMs are effective. We applied our models to automatic synthesis of the CPW geometries and capacitive couplers for branched multi-channel multi-port RF interconnect. We minimized the total interconnect area under the constraints of SNR and signal distortion. The solutions are verified with time-domain transient simulations. Compared to the published manual designs, the synthesized solutions can save up to 80% chip area. The complexity and large difference in the various optimized solutions demonstrate the necessity and effectiveness of our models and the automatic synthesis process.

5. REFERENCES

[1] R. T. Chang and et. al., "Near speed-of-light signaling over on-chip electrical interconnects," *IEEE J. Of Solid-State Circuits*, vol. 38, p. 834-838, 2003.

[2] M. Minzuno and et. al., "Clock distribution networks with on-chip transmission lines," in *Int'l Interconnect Technology Conf.*, 2000.

[3] M. F. Chang and et. al., "RF/wireless interconnect for inter- and intra-chip communications," *Proc. of the IEEE*, vol. 89, pp. 456–466, 2001.

[4] J. D. Warnock and et. al., "The circuit and physical design of the power4 microprocessor," *IBM J. of Research and Development*, vol. 46, p. 27-51, 2002.

[5] W. Ryu and et. al., "Over GHz low-power RF clock distribution for a multiprocessor digital system," *IEEE Trans. on Advanced Packaging*, vol. 25, pp. 18–27, 2002.

[6] R. Escovar and R. Suaya, "Transmission line design of clock trees," in *Proc. ICCAD*, 2002.

[7] B. M. Beckmann and D. A. Wood, "TLC: Transmission line caches," in *Int'l Symp. on Microarchitecture*, 2003.

[8] H. Shin and M. F. Chang, "1.1 Gbit/s RF-interconnect based on 10 GHz RF-modulation in 0.18 m CMOS," *Electronics Letters*, vol. 38, pp. 71–72, 2002.

[9] F. Y. Chang, "Waveform relaxation analysis of RLCG transmission lines," *IEEE Trans. on Circuits and Systems*, pp. 1394–1415, Nov 1990.

[10] A. Odabasioglu, C. M, and L. Pileggi, "PRIMA: Passive reduced-order interconnect macromodeling algorithm," *IEEE Trans. on Computer-Aided Design of Integrated Circuits and Systems*, 1998.

[11] J. A. Davis and J. D. Meindl, "Compact distributed RLC interconnect models. I. single line transient, time delay, and overshoot expressions," *IEEE Trans. on Electron Devices*, pp. 2068 –2077, November 2000.

[12] M. Kamon, M. Tsuk, and J. White, "Fasthenry: a multipole-accelerated 3d inductance extraction program," *IEEE Trans. on MIT*, 1994.

Table 3: Coupler and signal amplitude for ports

Port	1	2	3	4	5	6	7	8
Coupler (fF)	67	13	47	32	58	12	21	48
SPICE (mV)	-	14.8	8.9	9.9	8.7	14.5	9.0	-
Model (mV)	-	14.6	8.7	10.3	8.2	13.4	8.7	-
Error (%)	-	-1.3	-2.2	4.0	-5.7	-7.6	-3.3	-